RSC Advances

ROYAL SOCIETY OF CHEMISTRY

PAPER

View Article Online
View Journal | View Issue

Check for updates

Cite this: *RSC Adv.*, 2024, **14**, 3024

Effect of oxide impurities on the dissolution behavior of Th^{4+}, Be^{2+} and U^{4+} in fluoride salts

Yubing Yan,[ab] Yingjie Li,[ab] Haiying Fu,[a] Yuan Qian,[a] Qingnuan Li,[a] Qiang Dou*[ab] and Junxia Geng*[ab]

Received 13th December 2023
Accepted 28th December 2023

DOI: 10.1039/d3ra08506f

rsc.li/rsc-advances

Oxides are one of the most important impurities in the fuel salt of molten salt reactors (MSRs), and excessive oxide impurities pose a risk to the safe operation of MSRs. This study focused on investigating the precipitation behavior between Th^{4+}, U^{4+}, and Be^{2+} with O^{2-} in the 2LiF–BeF_2 (FLiBe) eutectic salt system. The results showed that the solubility of UO_2 was 5.52×10^{-3} mol kg^{-1}, and the solubility product (K_{sp}) of UO_2 was 6.14×10^{-7} mol^3 kg^{-3} in FLiBe salt at 650 °C. It was also found that the O^{2-} ion would firstly react with U^{4+} to form UO_2, and then the excessive O^{2-} would react with Be^{2+} to generate BeO in the FLiBe system. Despite conducting the solubility experiment of ThO_2 and titration experiment of FLiBe–ThF_4, the system failed to achieve the solubility and the K_{sp} of ThO_2. The main reason for this was that O^{2-} preferentially reacted with Be^{2+} over Th^{4+} to form precipitates, in other words, Be^{2+} exerted a protective effect against Th^{4+}. Above all, this work experimentally demonstrated that in the FLiBe system, O^{2-} preferentially combines with U^{4+} to form a precipitate, followed by Be^{2+}, while Th^{4+} is relatively inert.

Introduction

Reducing the use of fossil fuels seems to be an effective way to reduce CO_2 emissions and mitigate global warming, and many countries have chosen to develop sustainable nuclear power to partially replace traditional energy production.[1] Consequently, significant efforts have been made to develop nuclear energy, and one of the current efforts is to develop the fourth-generation advanced nuclear energy systems, such as molten salt reactors (MSRs). The characteristic of MSRs is the use of nuclear fuel in liquid form.[2–4] The fissile material (UF_4) and fertile material (ThF_4) are dissolved in the molten carrier salt, and several alternative fuel carrier salts are being considered, but the leading candidate is 2LiF–BeF_2 (FLiBe).[5–8] Using liquid fuel will give MSRs an excellent advantage in performing continuous on-line fuel purification. On-line refueling significantly reduces the costs associated with fuel fabrication. More importantly, the ability to perform on-line fuel processing makes MSR suitable for the use of thorium.

In molten salt reactors, the purities are critical for controlling of chemical problems in the molten salt and mitigating corrosion. Among them, oxide impurities are a particularly important contaminant in this regard, because they can cause serious problems, such as fuel deposition and corrosion of structural materials.[9–12] In addition to the impurities already present in the raw constituents of molten salt, partial oxide impurities are generated during reactor operation and maintenance. Water and oxygen are entrained in the gas phase of the reactor system, which are the major external sources of oxide impurities in MSRs; neutron irradiation of the fuel salt generates oxygen in the system during operation;[13] and some oxides can penetrate into the MSRs fuel from passive layers formed on the surface of the structural materials.[14] Although the oxide contamination in MSR is usually removed by sparging the molten salts with a mixture of H_2 and HF to control the oxygen content of the molten salt within an acceptable range,[15–19] after the molten salt is loaded into the reactor, oxide impurities will still be introduced slowly in the manner described above. Previous studies have shown that UF_4 in the fuel salt readily reacts with O^{2-} ions to form uranium oxide precipitates, as shown in eqn (2).[20,21] The formation of uranium precipitates would reduce the concentration of U^{4+} and cause the loss of fuel, what's more, the large accumulation of UO_2 precipitates on the structural metal surface of the primary circuit would create the overheated areas in the reactor, posing a potential threat to the reactor operation.

$$H_2O + 2F^- = 2HF + O^{2-} \quad (1)$$

$$UF_4 + 2O^{2-} = UO_2\downarrow + 4F^- \quad (2)$$

For the safety of the molten salt reactor, it is necessary to strictly control the concentration of O^{2-} in the fuel salt. In addition, the molten salt oxide chemistry of this research will

---

[a] Shanghai Institute of Applied Physics, Chinese Academy of Sciences, Shanghai, 201800, China. E-mail: gengjunxia@sinap.ac.cn; Tel: +86-21-39194027

[b] University of Chinese Academy of Sciences, Beijing 100049, China. E-mail: douqiang@sinap.ac.cn; Tel: +86-21-39190198

open the door to a deeper understanding of the precipitation and dissolution behavior of oxides in fluoride salts, which plays an important role in the chemical control of molten salt systems.

Studies of the dissolution and precipitation behaviors of UO_2 in fluoride salt have a long history, not least because of its importance in the safety of molten salt reactors. However, the existing studies showed a large scatter in the solubility product (K_{sp}) of UO_2, and the desired data are often not available due to the inappropriate experimental conditions such as the temperature and composition of molten salt. Peng *et al.*[20,22] have studied the precipitation of UO_2 in LiF–BeF$_2$ and LiF–NaF–KF fluoride salt systems at 600 °C, using electrochemical methods. Their study showed that the K_{sp} of UO_2 in the LiF–NaF–KF system was 4.75×10^{-6} mol^3 kg^{-3}, while in the LiF–BeF$_2$ system, it was 1.67×10^{-5} mol^3 kg^{-3}. There was an order of magnitude difference in the K_{sp} of UO_2 between the two systems. Oak Ridge National Laboratory (ORNL)[23] studied the K_{sp} of UO_2 in LiF–BeF$_2$–ThF$_4$–UF$_4$ at 500 °C, which was 2.60×10^{-7} mol^3 kg^{-3}. ORNL[24] has studied the system in detail and found that the K_{sp} of UO_2 at 600 °C in the LiF–BeF$_2$–ZrF$_4$ system was 1.20×10^{-5} mol^3 kg^{-3}. In LiF–BeF$_2$–UF$_4$ with the addition of 5% ZrF_4, Toth[25] found that Zr^{4+} had a greater binding interaction for O^{2-} than that of U^{4+}. This finding has led to an increased interest in studying the interaction between Zr^{4+} and O^{2-}, as Zr^{4+} can effectively integrate with O^{2-}. This property, combined with its small neutron absorption cross-section (thermal neutron absorption cross-section of 0.18 bar), has even led several researchers to advocate ZrF_4 as an ideal oxygen binding additive to prevent the precipitation of UO_2 in the fuel salt. Korenko[21] found that the introduction of oxide in the LiF–NaF–KF–UF$_4$–ZrF$_4$ system can generate ZrO_2 precipitation, which effectively consumed the O^{2-} in the molten salt and prevented the precipitation of UO_2. Studies of the LiF–BeF$_2$–ZrF$_4$–UF$_4$ system by Peng[26] showed that ZrO_2 formed initially as an O^{2-} addition of less than 1 mol kg^{-1}, with UO_2 and ZrO_2 co-precipitating at O^{2-} additions greater than 1 mol kg^{-1}. It implied that when oxide contamination exists in the melt containing both ZrF_4 and UF_4, a significant amount of ZrF_4 could inhibit the UO_2 formation. Later, Song and co-workers[27] found that in the system of LiF–BeF$_2$–ZrF$_4$–UF$_4$ system, when the molar ratio of Zr^{4+} to U^{4+} was greater than 4, only ZrO_2 precipitation formed after the quantitative addition of Li_2O. Conversely, ZrO_2 and UO_2 co-precipitated when the molar ratio was less than 4.

Thorium has been acknowledged as a marvelous resource for its potential application as nuclear fuel, it has been considered as a possible supplement or even a replacement for uranium. Therefore, it is crucial to study the chemical behavior of Th^{4+} in thorium-based molten salt reactors, as well as that of U^{4+}. Chamelot *et al.*[28] reported that the addition of oxides to LiF–CaF$_2$–ThF$_4$ produced the intermediate product ThOF$_2$, and gradually formed the ThO_2 with more O^{2-} added. Wang[29] used Raman spectroscopy to study the addition of Li_2O to FLiBe/FLiNaK–ThF$_4$ and found that there was stabilized $Th_2OF_{10}{}^{4-}$ anion with linear Th–O–Th geometry formed in both systems. Some related research on thorium utilization in molten salt reactors has been published over the years, despite the numerous investigations on the products and structures of thorium compounds, less effort has been dedicated to the precipitation and dissolution behavior of Th^{4+}.

The influence of O^{2-} ions on Th^{4+} and U^{4+} in the molten salt reactor has been proven to be significant. Researchers have attempted to establish an association between the precipitates of U^{4+}, Th^{4+}, and O^{2-}. It is necessary to have an understanding about the solubility and solubility product (K_{sp}) of ThO_2 and UO_2. Though a few studies have been performed for the solubility and K_{sp} of UO_2, the results obtained are inconclusive. Furthermore, to our knowledge, there is limited research about solubility and K_{sp} of ThO_2 has been performed so far. Therefore, this study concentrates on the interaction between O^{2-} and U^{4+}, Th^{4+}, as well as the precipitation and dissolution behavior of UO_2 and ThO_2 in the FLiBe system. This work aims to enhance knowledge of the oxide chemistry behavior in the FLiBe system.

Experiments

Solubility experiments of UO_2, ThO_2

The UO_2 and ThO_2 (applied by North China Nuclear Fuel Components Co., Ltd) powders were compressed into tablets, as shown in Fig. 1(a) and (b), and positioned at the bottom of the crucible respectively. Next, 20 g of FLiBe salt was used to cover the tablets. To prevent any interference with sampling, a piece of nickel mesh was placed between the FLiBe molten salt and UO_2/ThO_2 tablet to avoid powder diffusion. The UO_2 or ThO_2 was immersed in the FLiBe salt bath at 650 °C to create a saturated solution, which is illustrated in Fig. 2. Samples were taken hourly during the initial seven hours and subsequently every two hours. The samples were analyzed to determine the concentration of U^{4+} and Th^{4+} by ICP-OES, while the concentration of O^{2-} by LECO oxygen analyzer and ion chromatography. Based on the concentrations of U^{4+}/Th^{4+} and O^{2-} in salt samples, the solubility, as well as the solubility product (K_{sp}) can be calculated.

Preparation of FLiBe–ThF$_4$

In order to rapidly dissolve the ThF_4 (supplied by Changchun Institute of Chemical Engineering, with a purity of 99.9%) into the fluoride salt, it is necessary to synthesize a molten mixture of LiF and ThF_4 in advance. 10.2 g of ThF_4 was mixed with 2.8 g of LiF and melted at a temperature of 700 °C to prepare LiF–

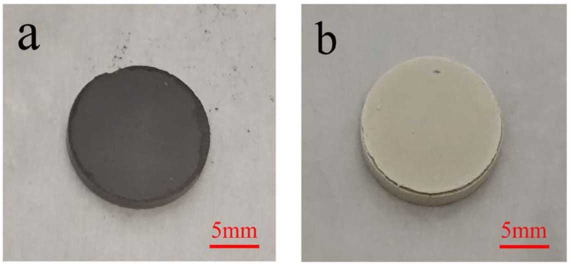

Fig. 1 (a) UO_2 after pressing; (b) ThO_2 after pressing.

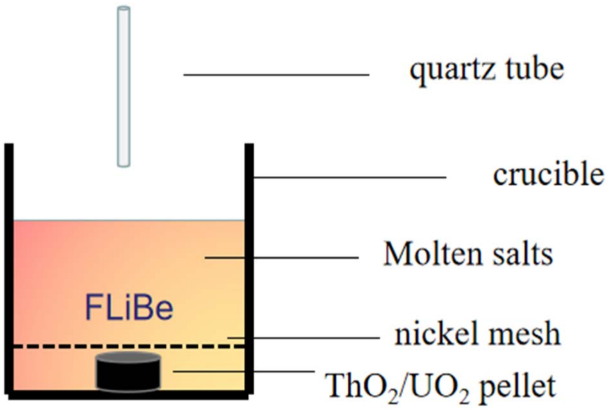

Fig. 2 Schematic diagram of solubility experiment of UO_2/ThO_2.

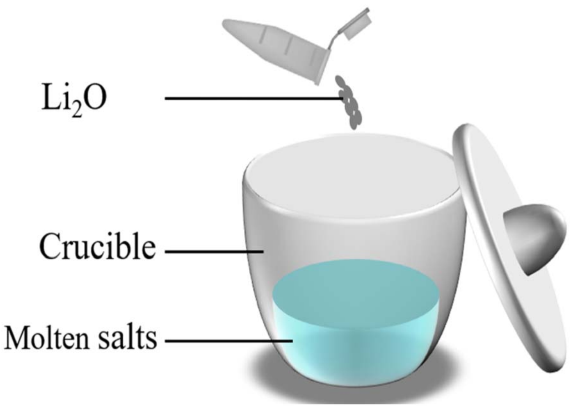

Fig. 3 Schematic diagram of FLiBe–UF_4/ThF_4 titration experiment.

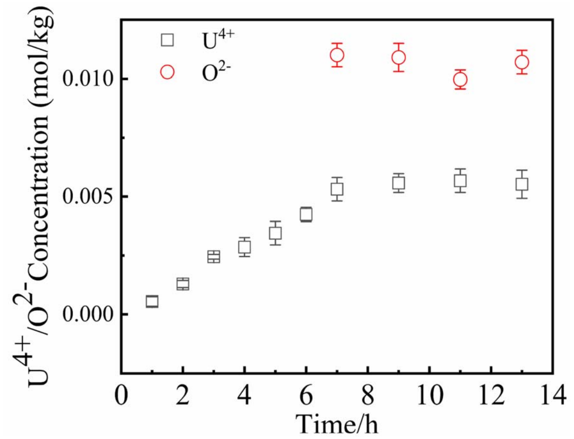

Fig. 4 Variation of U^{4+} and O^{2-} concentration with time at 650 °C.

ThF_4(FLiTh). The FLiTh was then mixed with FLiBe salt and heated to ensure that the ThF_4 uniformly dissolved into the FLiBe salt. The concentration of O^{2-} within the resulting FLiBe–ThF_4 mixture was determined to be 1.80×10^{-2} mol kg^{-1}.

Titration experiments of UF_4/ThF_4 with Li_2O in FLiBe

To investigate the reactions of U^{4+} and Th^{4+} with O^{2-} in the FLiBe system and obtain the corresponding values of K_{sp}, the titration experiments of UF_4/ThF_4 in FLiBe salt were carried out. In the titration experiment of FLiBe-UF_4, 1 g of UF_4 (supplied by China National Nuclear Corporation, Baotou No. 202 Plant, 99.9% purity) was mixed with 19 g of FLiBe molten salt in a crucible; in the titration experiment of FLiBe–ThF_4, 20 g of FLiBe–ThF_4 was used. O^{2-} ions were added to the melts in the form of Li_2O. After the O^{2-} was added, the salt mixture was stirred to ensure complete reaction of O^{2-} ions with U^{4+}/Th^{4+} ions in the salt (the schematic diagram is shown in Fig. 3). The temperature was maintained at 650 °C to allow the molten salt to settle, during the process, the supernatant was periodical extracted *via* a quartz tube for the concentration analysis of Th^{4+}, U^{4+} and O^{2-}.

Chemical analysis

The obtained samples were dissolved and diluted, and then the concentrations of cations (U^{4+}, Th^{4+}) in the molten salts were determined by ICP-OES (PerkinElmer Co., Ltd.). It was based on the premise that substances form a high-temperature plasma in a high-frequency electromagnetic field, so that the constituent elements of the compounds were generated into their excited states at high temperatures or by electric excitation, and that specific wavelengths of the electromagnetic spectral lines will be emitted when the elemental excited states were restored to the ground state, thus realizing qualitative or quantitative analyses of different samples.

The total concentration of O^{2-} in the experiment was measured with the LECO oxygen detector (LECO RO600, LECO Co., Ltd.). The obtained sample was ground into powder and weighed precisely, with approximately 0.05 g sample being wrapped in a tin capsule and placed in a graphite crucible. During the test process, the molten salt sample quickly went through the feeding platform into the graphite crucible, and then switched the current to heat the crucible to 2700 °C in a short period. At the high temperature, the molten salt samples were melted, causing a reaction between the oxygen contained

Table 1 Oxygen content in oxygenated anions and FLiBe molten salt

Total oxygen content of FLiBe, mol kg^{-1}	Oxygen content of oxygenated anions, mol kg^{-1}	Total oxygen content of oxygenated anions, mol kg^{-1}	O^{2-} content, mol kg^{-1}
8.56×10^{-3}	NO_3^- 1.56×10^{-3} PO_4^{3-} 2.13×10^{-3} SO_4^{2-} 3.56×10^{-3}	7.25×10^{-3}	1.31×10^{-3}

and carbon from the graphite crucible and generating CO and CO_2 gases. The generated gases entered the infrared cell and were detected using infrared absorption. The computer assimilated the detection signals of CO and CO_2 and subsequently calculated the total oxygen content value of the sample.

Weighed out about 0.1 g of sample into a PE bottle and added deionized water. The bottle was then put into an ultrasonic cleaner to extract the ions to be measured. Finally, the obtained liquid was quantitatively diluted and the oxygenated ions (NO_3^-, PO_4^{3-}, SO_4^{2-}) in the molten salt were determined using an ion chromatograph (ICS-2100, Dionex Co., Ltd).

Results and discussion

Content analysis of oxygen impurities in FLiBe salt

While the previous experiments and theoretical studies have focused on the oxygen impurity in fluoride salt, these results suggested that the oxygen impurities in the salt are composed of oxygen ions (O^{2-}) and oxygenated anions (including NO_3^-, PO_4^{3-}, SO_4^{2-} *etc.*).[22,30] During reactor operation and maintenance, the concentration of O^{2-} ions within the fuel system would increase gradually, which was attributed to moisture and oxygen leaking into the reactor and the corrosion of the passive layers of the structural materials. Different from O^{2-} ions, the oxygenated anions can be maintained at a relatively stable level, as oxygenated impurities were mainly introduced along with the carrier salt, LiF, BeF_2 and UF_4, *etc.*

The total oxygen content in the FLiBe molten salt was measured using a LECO oxygen analyzer. The oxygenated anions in molten salt were determined by ion chromatography. The practical O^{2-} concentration ($[O^{2-}]$) in molten fluorides was determined by subtracting the oxide concentration in oxygenated anions ($[O]_{IC}$) from the total oxide concentration ($[O]_{LECO}$), as shown in eqn (3). The measurement results of the total oxide concentration and the oxide concentration in oxygenated anions of FLiBe raw materials were listed in Table 1. The average total oxide concentration in the FLiBe molten salt was up to 8.56×10^{-3} mol kg^{-1}, as most of the oxygen and water contamination products were removed by sparging the salt with a mixture of H_2 and HF. The main oxygenated anions were found to be NO_3^-, PO_4^{3-}, and SO_4^{2-}. Based on the mass proportion of oxide in the oxygenated anion, the oxide concentrations in NO_3^-, SO_4^{2-}, and PO_4^{3-} were determined to have oxide concentrations of 1.56×10^{-3}, 2.13×10^{-3}, and 3.56×10^{-3} mol kg^{-1}, respectively. Thus, the resulting oxide concentrations in these three oxygenated anions were up to 7.25×10^{-3} mol kg^{-1}, and the O^{2-} content is then calculated to be 1.31×10^{-3} mol kg^{-1} using eqn (3).

$$[O^{2-}] = [O]_{LECO} - [O]_{IC} \tag{3}$$

Solubility of UO_2 in FLiBe salt

Since UO_2 has been proven to be the main precipitate of U^{4+} ions in the fuel system,[20] the key data of the solubility of UO_2 in FLiBe salt is of great significance for controlling the oxide content of the fuel salt. In this study, the solubility of UO_2 in FLiBe salt at a temperature of 650 °C was measured using the static dissolution method. UO_2 tablet were used in these dissolution experiments. Fig. 4 shows the changes of U^{4+} and O^{2-} concentrations in FLiBe salt as a function of dissolution time, where U^{4+} content in molten salt was regarded as the amount of UO_2 dissolved. It can be seen that the U^{4+} concentration kept increasing with an increase in dissolution time. Finally, as the dissolution time up to 7 hours, the $[U^{4+}]$ reached a final plateau with a constant concentration, thus indicating that 7 h was the dissolution equilibrium time. Furthermore, the solubility of UO_2 was calculated to be 5.52×10^{-3} mol kg^{-1}. It should be noted that, as shown in Fig. 4, there are no significant fluctuations in the O^{2-} concentration profile as dissolution periods greater than 7 hours. The average oxygen content was approximately 1.06×10^{-2} mol kg^{-1}, which is twice the U^{4+} equilibrium concentration, consistent with the U/O molar ratio in UO_2. Based on the concentration of O^{2-} and U^{4+} in FLiBe salt, the solubility product of uranium and oxygen ions (K'_{sp}) was determined to be 6.14×10^{-7} mol^3 kg^{-3}, as shown in Table 2.

Table 2 K_{sp} of UO_2 obtained from solubility experiment

	U^{4+}, mol kg^{-1}	Oxygen content, mol kg^{-1}	K'_{sp}, mol^3 kg^{-3}	Average value
1	5.31×10^{-3}	1.11×10^{-2}	6.54×10^{-7}	6.14×10^{-7}
2	5.57×10^{-3}	1.09×10^{-2}	6.07×10^{-7}	
3	5.67×10^{-3}	9.97×10^{-3}	5.64×10^{-7}	
4	5.52×10^{-3}	1.07×10^{-2}	6.32×10^{-7}	

Table 3 K_{sp} of different ratios of UO_2 (initial U^{4+} was 0.159 mol kg^{-1})

	Initial O^{2-}, mol kg^{-1}	Equilibrium U^{4+}, mol kg^{-1}	Equilibrium O^{2-}, mol kg^{-1}	K_{sp}, mol^3 kg^{-3}	Average value
O1–U	0.157	7.51×10^{-2}	9.31×10^{-3}	6.51×10^{-6}	3.80×10^{-6}
O2–U	0.316	9.61×10^{-3}	1.87×10^{-2}	3.36×10^{-6}	
O3–U	0.470	3.34×10^{-3}	2.13×10^{-2}	1.52×10^{-6}	

The titration of UF_4 with Li_2O in molten FLiBe

Understanding the impact of O^{2-} on the behavior of U^{4+} in fluoride salt not only has fundamental interests but also is important for reactor operation and maintenance. The K_{sp} of UO_2 is one of the most important parameters in the oxide chemistry of fuel salt, indicating the interaction between U^{4+} and O^{2-} ions. This study aimed to investigate the K_{sp} of UO_2 with different oxygen content by titrating UF_4 with Li_2O in FLiBe salt. Three sets of titration experiments were conducted with Li_2O/UF_4 ratios(molar ratio) of about 1 : 1, 1 : 2, and 1 : 3, which were called O1–U, O2–U and O3–U in this work, respectively. The equilibrium concentrations of U^{4+} and O^{2-} ions in molten FLiBe salt after each titration operation are given in Table 3. According to the data in Table 3, it was found that with an increase in the addition of Li_2O from 0.157 mol kg^{-1} to 0.470 mol kg^{-1}, the equilibrium concentrations of U^{4+} decreased sharply, while the equilibrium concentration of O^{2-} accordingly increased from 9.31×10^{-3} mol kg^{-1} to 2.13×10^{-2} mol kg^{-1}. Thus, based on the given data, the solubility product (K_{sp}) of U^{4+} and O^{2-} can be calculated to be 3.80×10^{-6} mol^3 kg^{-3}. This value was slightly greater than the K_{sp} obtained in the UO_2 solubility experiment. This may be attributed to some un-deposited UO_2 particles formed in the titration experiments, and these particles were picked up with the fluoride salt in the sampling process. The K_{sp} of UO_2 obtained from the experiment is compared with that in the literature, the results are shown in Table 4.

As seen in Table 3, there was a clear difference between the initial addition value and the equilibrium value of U^{4+} and O^{2-} in the melts. The concentration variation of the two ions in these titration experiments is shown in Fig. 5. Inspected in more detail, it was revealed that the variation in concentration of the $\Delta[U^{4+}]/\Delta[O^{2-}]$ ratio in the O1–U and O2–U experiments was about 1 : 2, consistent with the U/O molar ratio in UO_2. Fig. 6 shows the photographs of solidified FLiBe–UF_4 salts after the titration experiments. It was evident that distinct reddish-brown precipitate layers appeared at the bottom of the salts. Meanwhile, with an increase in the addition of Li_2O, the thickness of the precipitate layer increased, and the upper green molten salt gradually discolored. However, the results obtained in the O3–U experiment demonstrated that the $\Delta[U^{4+}]/\Delta[O^{2-}]$ ratio was approximately 1 : 2.9, which was different from the U/O molar ratio in UO_2. It was found that the $\Delta[U^{4+}]/\Delta[O^{2-}]$ ratio remained at 1 : 2.9 (shown in Table 5) upon repetition of the O3–U experiment.

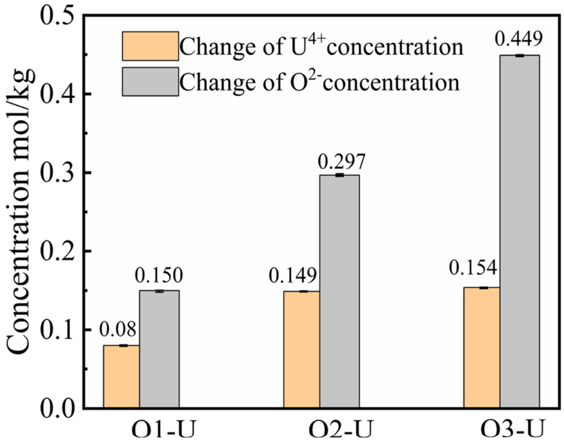

Fig. 5 Variation of U^{4+}, O^{2-} concentrations for experiments with different ratios.

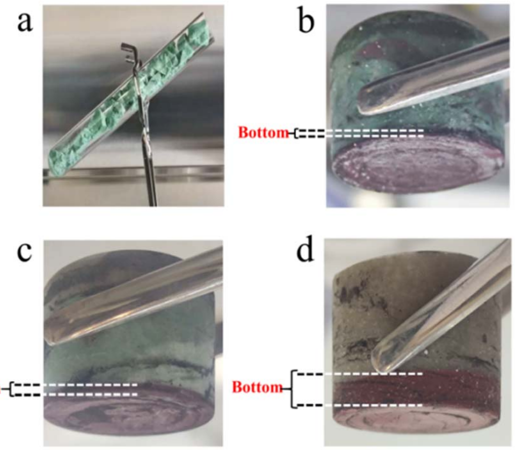

Fig. 6 (a) FLiBe-UF_4; (b) molten salt of O1–U; (c) molten salt of O2–U; (d) molten salt of O3–U.

XRD analysis was performed on the reddish-brown precipitate after most of the FLiBe salt was removed (shown in Fig. 7). The diffraction peaks on the XRD pattern indicated that all the precipitate layers in these titration experiments contain a large amount of UO_2. Later, these precipitates were analyzed by Raman spectrometer, and the analysis result (Fig. 8) showed that UO_2 was not the only generated precipitate in the O3–U experiment. Another insoluble oxide BeO[31] would form after

Table 4 K_{sp} of UO_2 in different molten salt systems

Molten salt system	Temperature/°C	K_{sp}/mol^3 kg^{-3}	Experimental condition
LiF–BeF_2	600	1.67×10^{-5}	Titration experiment
LiF–NaF–KF	600	4.75×10^{-6}	Titration experiment
LiF–BeF_2–ThF_4–UF_4	500	2.6×10^{-7}	Molten salt reactor
LiF–BeF_2–ZrF4	600	1.2×10^{-5}	Molten salt reactor
LiF–BeF_2	650	6.14×10^{-7}	Solubility experiment
LiF–BeF_2	650	3.80×10^{-6}	Titration experiment

Table 5 Concentration changes of U^{4+} and O^{2-} in the repeated experiment of O3–U

	Starting	Equilibrium	Variations	U^{4+}:O^{2-}percentage change
U^{4+} mol kg^{-1}	0.158	3.10×10^{-3}	0.155	1 : 2.9
O^{2-} mol kg^{-1}	0.469	2.35×10^{-2}	0.446	

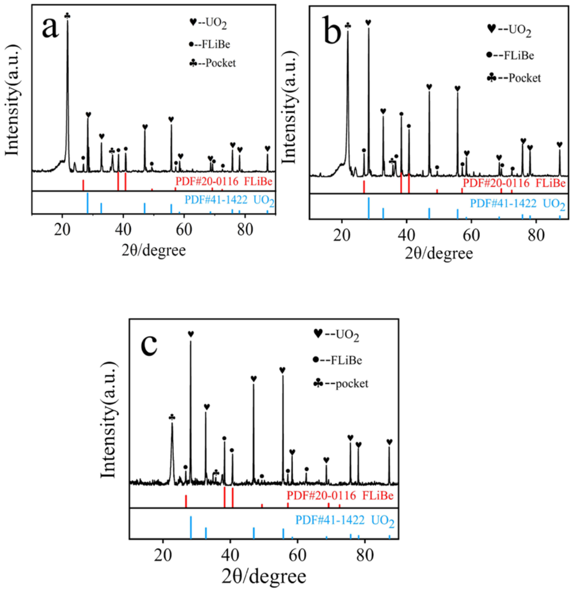

Fig. 7 (a) XRD analysis of the precipitate in O1–U; (b) XRD analysis of the precipitate in O2–U; (c) XRD analysis of the precipitate in O3–U.

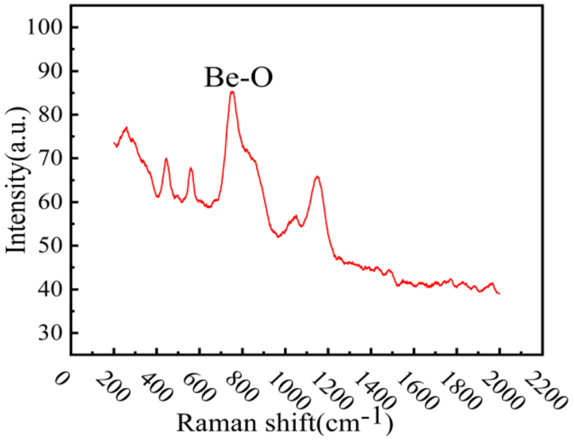

Fig. 8 Raman analysis of the precipitation in O3–U.

most U^{4+} ions were precipitated due to the successive addition of Li_2O. Such a result may explain the distinct deviation of the $\Delta[U^{4+}]/\Delta[O^{2-}]$ ratio in the O3–U experiment.

Solubility of ThO_2 in FLiBe salt

In MSRs using thorium, the deposition behavior of Th^{4+} is worthy of attention. Previous research have indicated that the Th^{4+} oxide precipitates in the form of ThO_2.[30] In order to study the precipitation and dissolution behavior of ThO_2 in the FLiBe system, the solubility of ThO_2 in molten FLiBe salt at 650 °C was studied by the static dissolution method. Fig. 9 presents the concentrations of Th^{4+} and O^{2-} in the molten salt at different times. The concentration of Th^{4+} increased from 1.24×10^{-3} mol kg^{-1} to 0.297 mol kg^{-1}, and did not reach dissolution equilibrium after 18 hours. However, the $[O^{2-}]$ fluctuated within a small range of 0.03 mol kg^{-1} after being dissolved for more than 10 hours, which was much less than the concentration of Th^{4+}. The variation of concentrations was not only inconsistent with the Th/O molar ratio in ThO_2 but also different from that of the UO_2 solubility experiment completely. Due to the continuous dissolution of Th^{4+} in FLiBe without reaching equilibrium during the experiment, the solubility and K_{sp} of ThO_2 could not be determined.

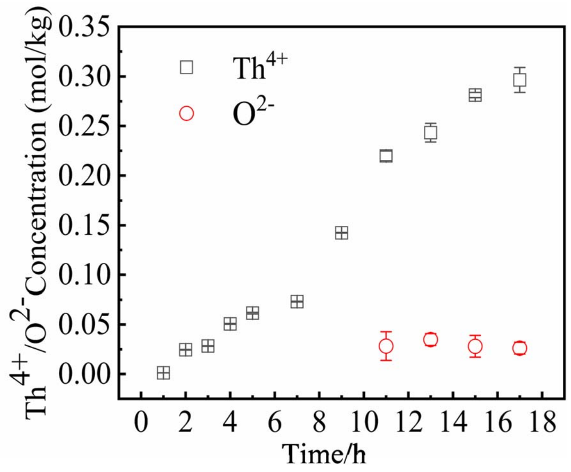

Fig. 9 Concentration changes of Th^{4+} and O^{2-} at 650 °C.

To explore why ThO_2 fails to reach its dissolution equilibrium just as UO_2 does, XRD analysis was conducted on the insoluble substance at the bottom of molten salt after removing

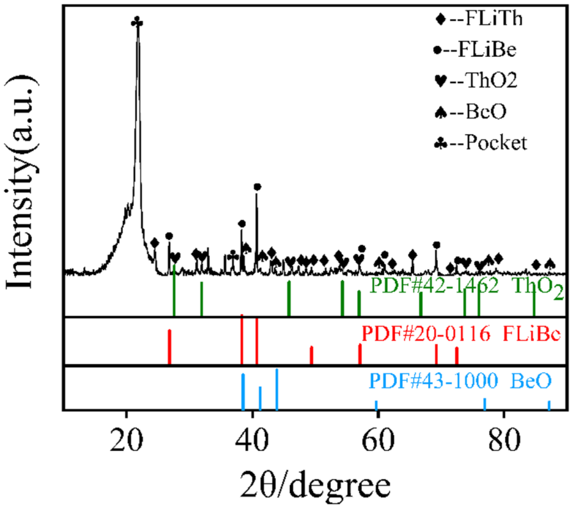

Fig. 10 Bottom precipitation XRD spectra of FLiBe–ThO_2 salt.

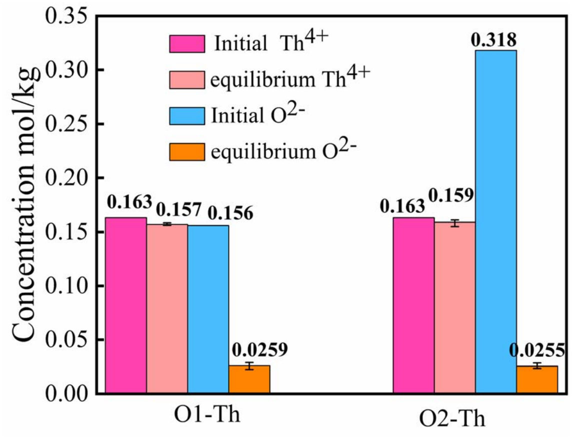

Fig. 11 Initial and equilibrium concentrations of Th^{4+} and O^{2-}.

Table 6 Concentrations of Th^{4+} ($Th^{4+} : O^{2-} = 1 : 2$)

	Th^{4+}, mol kg^{-1}
Upper part	0.160
Middle part	0.162
Lower part	0.157

the FLiBe salt by distillation. As shown in Fig. 10, it can be observed that BeO and ThO_2 coexisted. It was speculated that the O^{2-} generated from dissolved ThO_2 would react with Be^{2+}, which promoted the dissolution of ThO_2.

The titration of ThF_4 with Li_2O in molten FLiBe

It failed to get the K_{sp} of ThO_2 from the solubility experiment, which was extremely important to control the oxygen in molten salt, so the K_{sp} of ThO_2 was intended to be measured using the same method as the UO_2 titration experiment mentioned above. Two sets of titration experiments were conducted with Li_2O/ThF_4 ratio of about 1 : 1 and 1 : 2, denoted by O1–Th, O2–Th. Fig. 11 presents the initial and the equilibrium concentrations of Th^{4+}, O^{2-} in the molten salt, and shows a significant difference from the UO_2 titration experiment. As shown in this figure, with the addition of Li_2O, there was no obvious change in the concentration of Th^{4+}, while the $[O^{2-}]$ decreased unexpectedly. The result suggested that the introduction of O^{2-} may react with other cations, leading to the dissolution behavior of Th^{4+} to remain unaffected.

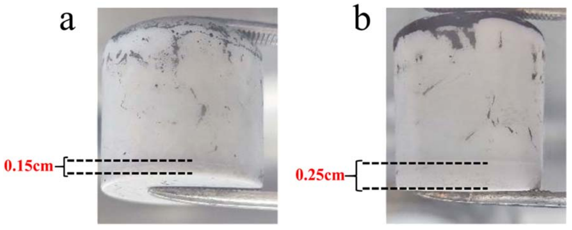

Fig. 12 (a) Molten salt of O1–Th; (b) molten salt of O2–Th.

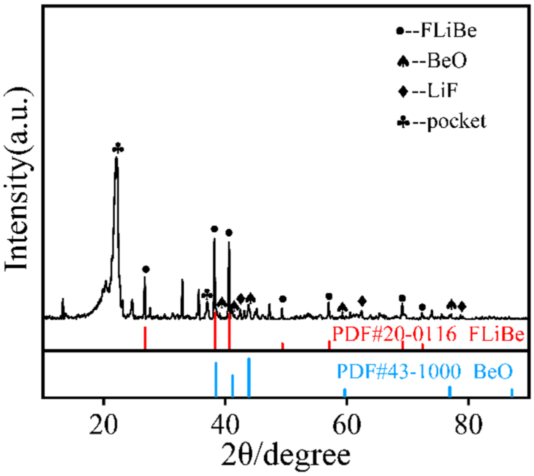

Fig. 13 XRD spectra of O2–Th bottom precipitation.

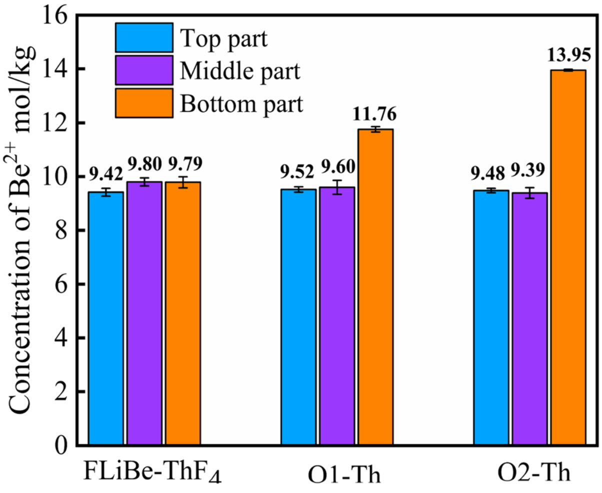

Fig. 14 Concentrations of Be^{2+} in FLiBe–ThF_4, O1–Th and O2–Th.

In order to determine whether the Th^{4+} in molten salt reacted with O^{2-}, the concentration of Th^{4+} in different sections of the molten salt of O2–Th was analyzed, the relevant result was shown in Table 6. It was evident that the concentrations of Th^{4+} in all three parts were similar, confirming that Th^{4+} was uniformly distributed in the FLiBe salt. However, obvious precipitates were observed at the bottom of the salt (as shown in Fig. 12), and the thickness of the precipitate layer increased

Table 7 Parallel measurement results of $[Th^{4+}]$, $[Be^{2+}]$, and $[O^{2-}]$ in FLiBe–ThF_4–BeO titration experiments (initial Th^{4+}, Be^{2+} were 0.163 and 9.67 mol kg^{-1}, respectively)

	Th^{4+}, mol kg^{-1}	Be^{2+}, mol kg^{-1}	O^{2-}, mol kg^{-1}
1	0.162	9.81	1.57×10^{-2}
2	0.160	9.62	1.75×10^{-2}
3	0.162	9.97	1.89×10^{-2}
4	0.161	9.61	1.89×10^{-2}

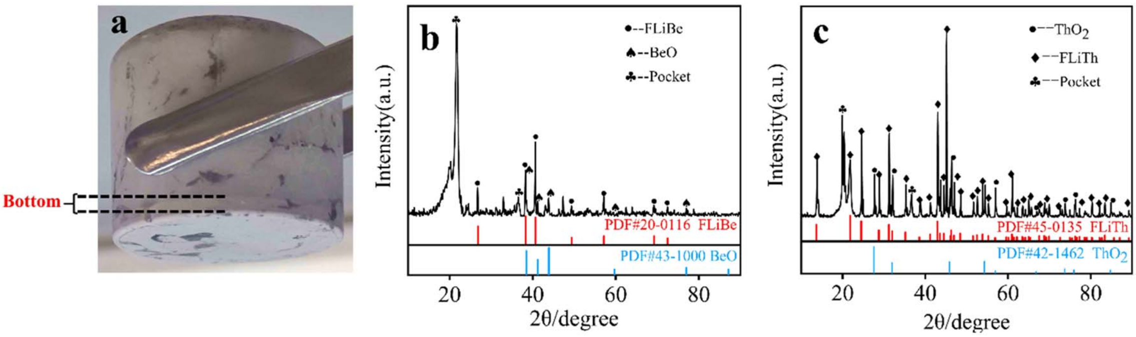

Fig. 15 (a) FLiBe–ThF_4–BeO molten salt; (b) XRD spectrum of the precipitation of FLiBe–ThF_4–BeO; (c) XRD spectrum of the precipitation of FLiTh–Li_2O.

with the increase of O^{2-}. Subsequently, an XRD analysis was performed on the precipitate after most of FLiBe salt was removed (Fig. 13). The XRD pattern confirmed the presence of BeO but no ThO_2 in the precipitate.

Therefore, it is necessary to determine the concentration of Be^{2+} in the molten salt. Fig. 14 illustrates the variation of $[Be^{2+}]$ at different sections within the molten salts of O1–Th, O2–Th, and FLiBe–ThF_4. It can be seen that the $[Be^{2+}]$ remained relatively consistent across different positions in the FLiBe–ThF_4 molten salt. However, in the salts of O1–Th and O2–Th, the $[Be^{2+}]$ at the bottom was higher than that of the top and middle sections. Furthermore, the $[Be^{2+}]$ at the bottom of O2–Th was higher than that of O1–Th. These experimental findings suggested that the addition of O^{2-} led to an enrichment of Be^{2+} at the bottom, which could be attributed to the fact that O^{2-} did not react with Th^{4+} but with Be^{2+} in the FLiBe system.

The comparison of binding ability of Th^{4+}, Be^{2+} with O^{2-} in fluoride salts

Based on the titration experiments results outlined above, two sets of experiments were specifically designed to investigate the interaction between Be^{2+}, Th^{4+} and O^{2-} in fluoride salts. To observe whether the Th^{4+} has the ability to capture the O^{2-} from BeO, the titration experiment of ThF_4 in the FLiBe was conducted by adding BeO instead of Li_2O. And to examine whether O^{2-} can combine with Th^{4+} to generate ThO_2, the titration experiment of ThF_4 with Li_2O in FLiTh without Be^{2+} was performed.

In the titration experiment of ThF_4 with BeO in FLiBe, the ratio of BeO/ThF_4 was set to be 1 : 2. The equilibrium $[Th^{4+}]$ and $[Be^{2+}]$ as well as the $[O^{2-}]$ in the supernatant of the molten salt were listed in Table 7. It showed that there was no obvious change in the concentrations of Be^{2+}, Th^{4+} and O^{2-}. However, Fig. 15(a) presents obvious precipitation at the bottom of the molten salt, and XRD characterization (the result shown in Fig. 15(b)) revealed that the precipitation was BeO. The experimental results confirmed that the BeO did not react with Th^{4+} in FLiBe molten salt, suggesting it is difficult for Th^{4+} to capture the O^{2-} in BeO.

In another titration experiment of ThF_4, Li_2O was directly added to FLiTh salt, and the precipitate obtained in this system was characterized by XRD after the removal of the molten salt (shown in Fig. 15(c)). The XRD pattern clearly revealed the presence of ThO_2, indicating that Th^{4+} has the ability to react with O^{2-} to form ThO_2 in the absence of Be^{2+}.

Based on the solubility experiment of ThO_2 and the titration experiment of ThF_4 in FLiBe salt, it was clearly demonstrated that when O^{2-} was introduced into the FLiBe–ThF_4 salt, it preferentially reacted with Be^{2+} rather than Th^{4+}. This suggested that Be^{2+} had a protective effect on Th^{4+} in the fluoride salt system.

Conclusions

To investigate the effect of O^{2-} on the fuel salt of molten salt reactor, and provide a basis for understanding the chemical behavior of oxides in the fluoride salt system, this study focused on the solubility of UO_2 and ThO_2, as well as the interaction behavior of O^{2-} with U^{4+}, Th^{4+}, and Be^{2+} in the FLiBe system. The main findings are summarized as follows.

(1) At a temperature of 650 °C, the solubility of UO_2 was 5.52×10^{-3} mol kg^{-1}, and the value of K_{sp} was 6.14×10^{-7} mol^3 kg^{-3}. When the added $[O^{2-}]$ was less than twice of the $[U^{4+}]$ in the FLiBe system, O^{2-} would preferentially react with U^{4+} to form UO_2 precipitate. As more O^{2-} continued to be introduced, O^{2-} would react with Be^{2+} to generate BeO precipitate.

(2) When O^{2-} was introduced into the FLiBe–ThF_4 system, O^{2-} would preferentially react with Be^{2+} rather than Th^{4+}, and only in the absence of Be^{2+}, O^{2-} reacted with Th^{4+} to form ThO_2. In brief, O^{2-} introduced into the FLiBe molten salt at 650 °C would react firstly with U^{4+}, then with Be^{2+}, and finally with Th^{4+}.

Hence, when oxide impurities were introduced into the molten salt reactor fuel, it is important to take into account their impact on uranium to prevent the formation of UO_2 precipitate. The current results indicated that the presence of a large number of U^{4+} and Be^{2+} played a certain protective role for Th^{4+}.

Author contributions

Yubing Yan: methodology, investigation, writing – original draft, writing – review. Yingjie Li: data curation, investigation.

Haiying Fu: conceptualization, methodology. Yuan Qian: conceptualization. Qingnuan Li: conceptualization, validation. Junxia Geng: writing – review, supervision, validation. Qiang Dou: writing – review, validation, project administration, resources.

Conflicts of interest

There are no conflicts to declare.

Acknowledgements

This work was supported by the National Natural Science Foundation of China (No. 12175303 and U2267226), Xinjiang Uygur Autonomous Region Key R&D Task Special Project (No. 2022B01039).

References

1 L. Mathieu, D. Heuer, R. Brissot, C. Garzenne, C. L. Brun, D. Lecarpentier, E. Liatard, A. Nuttin, E. Walle and J. Wilson, *Prog. Nucl. Energy*, 2006, **48**, 664–679.

2 C. György and Sz. Czifrus, *Prog. Nucl. Energy*, 2016, **93**, 306–317.

3 J. Serp, M. Allibert, S. Delpech, O. Feynberg, V. Ghetta, D. Heuer, D. Holcomb, V. Ignatiev, J. L. Kloosterman, L. Luzzi, R. Yoshioka and D. Zhimin, *Prog. Nucl. Energy*, 2014, **77**, 308–319.

4 O. Benes and R. J. M. Konings, *J. Fluorine Chem.*, 2009, **130**, 22–29.

5 P. Souček, O. Beneš, B. Claux, E. Capelli, M. Ougier, V. Tyrpekl, J. F. Vigier and J. M. Konings, *J. Fluorine Chem.*, 2017, **200**, 33–40.

6 C. Forsberg, *Prog. Nucl. Energy*, 2005, **47**, 32–43.

7 A. Nuttin, D. Heuer, A. Billebaud, R. Brissot, C. Le Brun, E. Liatard, J. M. Loiseaux, L. Mathieu, O. Meplan and E. M. Lucotte, *Prog. Nucl. Energy*, 2005, **46**, 77–99.

8 M. L. Tan, G. F. Zhu, Z. D. Zhang, Y. Zou, X. H. Yu, C. G. Yu, Y. Dai and R. Yan, *Nucl. Sci. Technol.*, 2022, **33**, 5.

9 H. Nishimura, T. Terai, T. Yoneoka, S. Tanaka, A. Sagara and O. Motojima, *J. Nucl. Mater.*, 2000, **283–287**, 1326–1331.

10 Y. L. Wang, Q. Wang, H. J. Liu and C. L. Zeng, *Corros. Sci.*, 2016, **103**, 268–282.

11 F. Y. Ouyang, C. H. Chang, B. C. You, T. K. Yeh and J. J. Kai, *J. Nucl. Mater.*, 2013, **437**, 201–207.

12 K. M. Sankar and P. M. Singh, *Corros. Sci.*, 2022, **206**, 110473.

13 S. Q. Guo, J. S. Zhang, W. Wu and W. T. Zhou, *Prog. Mater. Sci.*, 2018, **97**, 448–487.

14 N. J. Condon, S. Lopykinski, F. Carotti, K. E. Johnson and A. Kruizenga, *ACS Omega*, 2023, **8**, 29789–29793.

15 R. D. Scheele, A. M. Casella and B. K. McNamara, *Ind. Eng. Chem. Res.*, 2017, **56**, 5505–5515.

16 D. A. Petti, G. R. Smolik, M. F. Simpson, J. P. Sharpe, R. A. Anderl, S. Fukada, Y. Hatano, M. Hara, Y. Oya, T. Terai, D. K. Sze and S. Tanaka, *Fusion Eng. Des.*, 2006, **81**, 1439–1449.

17 A. L. Mathews and C. F. Baes Jr, *Inorg. Chem.*, 1968, **7**, 373–382.

18 P. Calderoni, P. Sharpe, H. Nishimura and T. Terai, *J. Nucl. Mater.*, 2009, **386–388**, 1102–1106.

19 S. Delpech, C. Cabet, C. Slim and G. S. Picard, *Mater. Today*, 2010, **13**, 34–41.

20 H. Peng, M. Shen, Y. Zuo, X. X. Tang, R. Tang and L. D. Xie, *Electrochim. Acta*, 2016, **222**, 1528–1537.

21 M. Korenko, M. Straka, J. Uhlíř, L. Szatmáry, M. Ambrová and M. Šimurda, *J. Radioanal. Nucl. Chem.*, 2014, **302**, 549–554.

22 H. Peng, W. Huang, L. D. Xie and Q. N. Li, *J. Nucl. Mater.*, 2020, **531**, 152004.

23 *Molten-salt Reactor Program: the Development Status of Molten-Salt Breeder Reactors*, ORNL-4812, 1972.

24 *Molten-salt Reactor Program: Semiannual Progress Report for Period Ending*, ORNL-3419, 1963.

25 L. Toth, U. Gat, G. Del Cul, S. Dai and D. Williams, *Review of ORNL's MSR technology and status*, Oak Ridge National Lab., 1996.

26 H. Peng, Y. L. Song, N. Ji, L. D. Xie, W. Huang and Y. Gong, *RSC Adv.*, 2021, **31**, 18708–18716.

27 Y. L. Song, M. Shen, S. F. Zhao, R. Tang, L. D. Xie and Y. Qian, *J. Electrochem. Soc.*, 2021, **168**, 036513.

28 P. Chamelot, L. Massot, L. Cassayre and P. Taxil, *Electrochim. Acta*, 2010, **55**, 4758–4764.

29 C. Y. Wang, X. T. Chen and Y. Gong, *J. Phys. Chem.*, 2021, **125**, 1640–1646.

30 M. Y. Xie, L. Li, Y. P. Ding and G. X. Zhang, *J. Nucl. Mater.*, 2017, **487**, 317–322.

31 S. M. Lee, Y. Jiang, J. Jung, J. H. Yum, E. S. Larsen, C. W. Bielawski, W. Wang, J. H. Ryoue, H. S. Kimf, H. Y. Chaf and J. Oh, *Appl. Surf. Sci.*, 2019, **469**, 634–640.